



Universidad Autónoma
de Madrid

Biblos-e Archivo
Repositorio Institucional UAM

Repositorio Institucional de la Universidad Autónoma de Madrid

<https://repositorio.uam.es>

Esta es la **versión de autor** del artículo publicado en:
This is an **author produced version** of a paper published in:

IEEE Transactions on Antennas and Propagation 71.8 (2023): 6989 - 6994

DOI: <https://doi.org/10.1109/TAP.2023.3285364>

Copyright: © 2023 IEEE

El acceso a la versión del editor puede requerir la suscripción del recurso
Access to the published version may require subscription

Communication

Leveraging Symmetry in the Analysis of Mirror-Symmetric Multilayered Periodic Structures with Application to LP-to-CP Converter Design

Miguel Camacho, *Member, IEEE*, Rafael R. Boix, *Member, IEEE*, Juan Córcoles, *Senior Member, IEEE*, and Francisco Medina, *Fellow, IEEE*

Abstract—This communication proves that the analysis of the scattering by a mirror-symmetric multilayered periodic structure can be replaced by the analysis of the scattering by two semi-structures with half the size in which the symmetry plane behaves either as a perfect magnetic conductor (PMC) or as a perfect electric conductor (PEC). The proof is based on the reflection properties of the electric and magnetic fields through PMCs and PECs, and it is valid for arbitrary oblique incidence. As an application of this concept, the spectral domain Method of Moments (SD-MoM) is reformulated to deal with MPSs limited by PMCs and PECs, and it is used in the design of a mirror-symmetric multilayered linear to circular polarization (LP-to-CP) converter. The results obtained with SD-MoM are validated by comparison with commercial software CST. Numerical simulations show that the CPU time required by both SD-MoM and CST in the analysis of half the LP-to-CP converter limited by PMC and PEC is between 30 and 42 per cent smaller than that required by the analysis of the complete LP-to-CP converter, which shows the numerical advantage gained in exploiting the symmetry when it is present.

Index Terms—Multilayered media, periodic structures, polarization conversion.

I. INTRODUCTION

Multilayered periodic structures (MPSs) with embedded arrays of conducting patches or/and apertures are known for their frequency selective and polarization selective properties.

In particular, MPSs acting as frequency selective surfaces (FSSs) have been used as spatial filters at microwave frequencies [1], [2]. Although the first prototypes of FSSs were built with a single metallization level, it soon became apparent that the use of multilayered structures with different metallization levels of patches and apertures enabled a larger bandwidth and a sharper frequency selectivity as demonstrated in [3]–[7]. Many of these MPSs with several metallization levels contain a mirror symmetry plane since their design is based on filtering equivalent circuits that are symmetric by nature.

Also, MPSs have become a low-profile low-cost approach for the design of linear polarization (LP) to circular polar-

ization (CP) converters. Since the design of CP antennas is challenging, the combined use of an LP antenna and an LP-to-CP converter is a good solution for a CP antenna, decoupling the problem of the antenna design from the problem of generating CP waves. As in the case of FSSs, LP-to-CP converters can be made of MPSs with several metallization levels since this introduces enough degrees of freedom to achieve either broadband performance [8]–[11] or dual band performance [12], [13], and to achieve a stable behavior for large angles of incidence [8], [10], [13]. Also, as in FSSs, the MPSs used for LP-to-CP conversion possess a mirror symmetry plane [8]–[13].

Mirror-symmetric MPS may have either an even number [6], [8], [11], [12] or an odd number [7], [9], [10] of metallization levels. In the latter case, the symmetry plane coincides with the middle metallization level. An MPS with an odd number of metallization levels can be always converted into an MPS with an even number of metallization levels by splitting the middle metallization level into two closely spaced metallization levels with the same metallization pattern separated by a bonding layer (see Fig. 7 of [8]). In practice, this splitting of the middle metallization level is required to maintain the symmetry in the manufacturing process due to the need for bonding layers (or prepreg layers) in the assembly of the MPS [8].

This communication first shows that the analysis of a mirror-symmetric MPS with an even number of metallization levels of the type used in high performance FSSs and LP-to-CP converters can be split into the analysis of two MPSs with half the thickness in which the symmetry plane behaves either as a perfect magnetic conductor (PMC) or as a perfect electric conductor (PEC). In analogy with microwave circuit theory, the excitation in the presence of a PMC symmetry plane (magnetic wall) would correspond to the even mode excitation, while considering a PEC symmetry plane (electric wall) would yield the odd mode excitation [14]. Since equivalent circuits with transmission lines have been used for the modelling of MPS under normal incidence [3], [8], [11]–[13], one could suspect of the direct extrapolation of the even-odd mode analysis under normal incidence conditions. However, the novelty of the theory presented in this work is that the even-odd mode analysis is proven to be valid not only for normal incidence but also for any arbitrary oblique incidence.

Next, this communication adapts a highly efficient spectral-domain Method of Moments (SD-MoM) formulation focused on MPS analysis [7] to account for PMC or PEC boundary conditions. To do so, the spectral-domain dyadic Green's function has to be re-derived in the presence of a PMC and a PEC,

This work was supported by Grant PID2020-116739GB-I00 funded by MCIN/AEI/ 10.13039/501100011033. The work of J. Córcoles was supported by Grant CA2/RSUE/2021-00325 funded by the Spanish Ministry of Universities, PRTR and UAM, and by Grants PID2020-116968RB-C32 and TED2021-130650B-C21 funded by MCIN/AEI/ 10.13039/501100011033 and by European Union "NextGenerationEU"/PRTR.

M. Camacho, R. R. Boix and F. Medina are with the Microwaves Group, Department of Electronics and Electromagnetism, College of Physics, University of Seville, 41012 Seville, Spain (e-mails: mcamachoa@us.es; boix@us.es; medina@us.es)

J. Córcoles is with the Department of Electronic and Communications Technology, School of Engineering (Escuela Politécnica Superior), Universidad Autónoma de Madrid, 28049 Madrid, Spain (e-mail: juan.corcoles@uam.es).

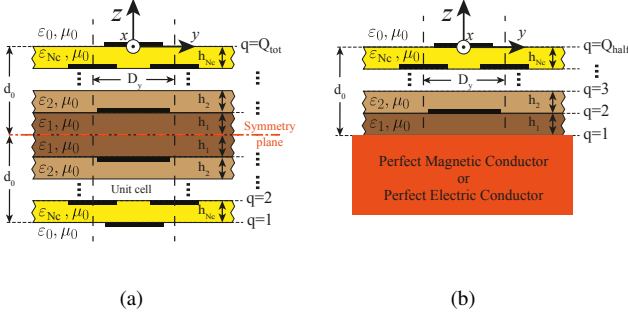


Fig. 1. (a) MPS with symmetry plane. (b) The MPS of (a) in the cases where the symmetry plane behaves either as a PMC or as a PEC.

which is a topic that was tackled in the past in the frame of the analysis of planar transmission lines for microwave circuits [15], but has not received any attention when addressing the analysis of the scattering by MPSs for antenna applications (FSSs, LP-to-CP converters, transmitarrays, etc.). Finally, by using a code based on the analysis of two semi-MPSs with PMC and PEC, we carry out a full-wave design of an LP-to-CP converter with six metallization levels of the type described in [8]. The results obtained show excellent agreement with results provided by commercial software CST (used for validation purposes). The CPU times required by both the SD-MoM and CST in the analysis of the two semi-MPSs with PMC and PEC are about one third of those required by the analysis of the complete LP-to-CP converter, which shows the benefit of exploiting symmetry in the numerical analysis of mirror-symmetric MPSs.

II. THEORETICAL FORMULATION

A. Scattering by an MPS with a symmetry plane

Fig. 1(a) shows an MPS with a symmetry plane. We will assume that the unit cell of the MPS is a rectangle of dimensions $D_x \times D_y$. Also, we will assume that the $2N_c$ layers of the multilayered medium have a thickness h_i , an electric permittivity $\epsilon_i = \epsilon_0 \epsilon_{ri}$ (which can be complex-valued to account for dielectric losses) and a magnetic permeability μ_0 , as shown in Fig. 1(a). Conductor losses will be neglected in the metallizations. In the following, we will assume that the electromagnetic fields existing in the MPS show a time dependence of the type $e^{j\omega t}$, which will be suppressed throughout.

Let us assume that the symmetry plane of the MPS of Fig. 1(a) behaves as a PMC, so that the semi-MPS to be analyzed corresponds to the PMC-case shown in Fig. 1(b). Let us also assume that a plane wave impinges on the semi-MPS from the upper half-space $z > 0$ in a direction given by the angular spherical coordinates θ_{inc} and φ_{inc} . The electric field of the incident wave $\mathbf{E}_{\text{inc}}^{\text{up}}(\mathbf{r})$, and the magnetic field of the incident wave, $\mathbf{H}_{\text{inc}}^{\text{up}}(\mathbf{r})$, can be written as

$$\mathbf{E}_{\text{inc}}^{\text{up}}(\mathbf{r}) = \frac{1}{2} (E_{0x}^i \hat{\mathbf{x}} + E_{0y}^i \hat{\mathbf{y}} + E_{0z}^i \hat{\mathbf{z}}) e^{-j\mathbf{k}_{\text{inc}} \cdot \mathbf{r}} \quad (1)$$

$$\mathbf{H}_{\text{inc}}^{\text{up}}(\mathbf{r}) = \frac{1}{2} (H_{0x}^i \hat{\mathbf{x}} + H_{0y}^i \hat{\mathbf{y}} + H_{0z}^i \hat{\mathbf{z}}) e^{-j\mathbf{k}_{\text{inc}} \cdot \mathbf{r}} \quad (2)$$

where $\mathbf{k}_{\text{inc}} = -k_0(\sin \theta_{\text{inc}} \cos \varphi_{\text{inc}} \hat{\mathbf{x}} + \sin \theta_{\text{inc}} \sin \varphi_{\text{inc}} \hat{\mathbf{y}} + \cos \theta_{\text{inc}} \hat{\mathbf{z}})$ is the wave vector of the incident wave, and k_0

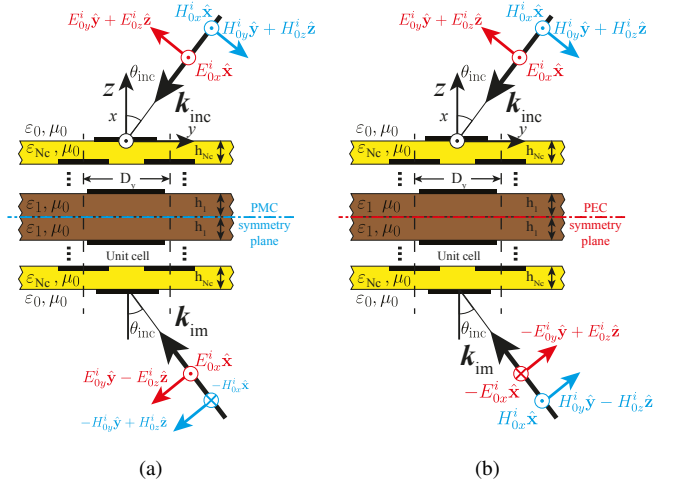


Fig. 2. (a) A plane wave impinges on an MPS with symmetry plane from the upper half-space $z > 0$ in the case where the symmetry plane behaves as a PMC (magnetic wall). (b) The situation of (a) when the symmetry plane behaves as a PEC (electric wall).

is the wavenumber in free space. Please note that (1)-(2) and the expression for \mathbf{k}_{inc} are general, in the sense that no assumption is made regarding the polarization or the incident direction (normal or oblique) for the impinging wave. In this case, the components of the electric field parallel to a PMC have a mirror image of the same sign, and the component of the electric field normal to a PMC has a mirror image of opposite sign. Also, the components of the magnetic field have mirror images through the PMC of opposite sign to those of the electric field. In accordance with these two latter statements, the presence of the incident wave from the upper half-space $z > 0$ will cause an *image* incident wave [16] impinging on the MPS from the lower half space $z < -2d_0$, as shown in Fig. 2(a), for which the electric field, $\mathbf{E}_{\text{im}}^{\text{PMC}}(\mathbf{r})$, and the magnetic field, $\mathbf{H}_{\text{im}}^{\text{PMC}}(\mathbf{r})$ have the following expressions

$$\mathbf{E}_{\text{im}}^{\text{PMC}}(\mathbf{r}) = \frac{1}{2} (E_{0x}^i \hat{\mathbf{x}} + E_{0y}^i \hat{\mathbf{y}} - E_{0z}^i \hat{\mathbf{z}}) e^{-j\mathbf{k}_{\text{im}} \cdot \mathbf{r}} \quad (3)$$

$$\mathbf{H}_{\text{im}}^{\text{PMC}}(\mathbf{r}) = \frac{1}{2} (-H_{0x}^i \hat{\mathbf{x}} - H_{0y}^i \hat{\mathbf{y}} + H_{0z}^i \hat{\mathbf{z}}) e^{-j\mathbf{k}_{\text{im}} \cdot \mathbf{r}} \quad (4)$$

where the wave vector of the *image* incident wave is given by $\mathbf{k}_{\text{im}} = -k_0(\sin \theta_{\text{inc}} \cos \varphi_{\text{inc}} \hat{\mathbf{x}} + \sin \theta_{\text{inc}} \sin \varphi_{\text{inc}} \hat{\mathbf{y}} - \cos \theta_{\text{inc}} \hat{\mathbf{z}})$.

Now, let us assume the incident plane wave given by (1)-(2) impinges from the upper half-space $z > 0$ on the semi-MPS of Fig. 1(b) for the PEC-case (i.e., the symmetry plane of the mirror-symmetric MPS of Fig. 1(a) behaves as a PEC). As in the previous case, there is also an *image* incident wave [16] impinging on the MPS from the lower half space $z < -2d_0$, as shown in Fig. 2(b). Since the electric and magnetic fields reflect through a PEC with signs opposite to those of their reflection through a PMC, the electric and magnetic field of the *image* incident wave are given by

$$\mathbf{E}_{\text{im}}^{\text{PEC}}(\mathbf{r}) = -\mathbf{E}_{\text{im}}^{\text{PMC}}(\mathbf{r}); \quad \mathbf{H}_{\text{im}}^{\text{PEC}}(\mathbf{r}) = -\mathbf{H}_{\text{im}}^{\text{PMC}}(\mathbf{r}) \quad (5)$$

Let us now add the two excitations of the MPS in the presence of the PMC and PEC symmetry planes of Figs. 2(a) and 2(b). According to (1)-(5), the total impinging fields

existing in the upper half-space ($\mathbf{E}_{\text{inc}}(\mathbf{r})$, $\mathbf{H}_{\text{inc}}(\mathbf{r})$) and the lower half-space ($\mathbf{E}_{\text{im}}(\mathbf{r})$, $\mathbf{H}_{\text{im}}(\mathbf{r})$) of the mirror-symmetric MPS of Fig. 1(a) will be

$$\mathbf{E}_{\text{inc}}(\mathbf{r}) = 2\mathbf{E}_{\text{inc}}^{\text{up}}(\mathbf{r}), \mathbf{H}_{\text{inc}}(\mathbf{r}) = 2\mathbf{H}_{\text{inc}}^{\text{up}}(\mathbf{r}), \quad z > 0 \quad (6)$$

$$\mathbf{E}_{\text{im}}(\mathbf{r}) = \mathbf{0}, \quad \mathbf{H}_{\text{im}}(\mathbf{r}) = \mathbf{0}, \quad z < -2d_0 \quad (7)$$

By assuming that the dimensions of the unit cell D_x and D_y prevent grating lobes from being excited [2], under excitations (6)-(7) the only wave scattered by the MPS of Fig. 1(a) in the far-field of the upper half-space $z > 0$ is that reflected in the specular direction. If we use the superposition principle, the complex amplitudes of the components of the electric field of this reflected wave parallel to the symmetry plane in Fig. 1(a) (E_{0x}^r, E_{0y}^r) can be obtained in terms of the complex amplitudes of the components of the incident electric field parallel to the symmetry plane (E_{0x}^i, E_{0y}^i) by means of the expression

$$\begin{pmatrix} E_{0x}^r \\ E_{0y}^r \end{pmatrix} = \bar{\mathbf{R}}_{\text{PMC}} \cdot \begin{pmatrix} \frac{1}{2}E_{0x}^i \\ \frac{1}{2}E_{0y}^i \end{pmatrix} + \bar{\mathbf{R}}_{\text{PEC}} \cdot \begin{pmatrix} \frac{1}{2}E_{0x}^i \\ \frac{1}{2}E_{0y}^i \end{pmatrix} \\ = \left(\frac{1}{2}\bar{\mathbf{R}}_{\text{PMC}} + \frac{1}{2}\bar{\mathbf{R}}_{\text{PEC}} \right) \cdot \begin{pmatrix} E_{0x}^i \\ E_{0y}^i \end{pmatrix} = \bar{\mathbf{R}} \cdot \begin{pmatrix} E_{0x}^i \\ E_{0y}^i \end{pmatrix} \quad (8)$$

where $\bar{\mathbf{R}}_{\text{PMC}}$ is the reflection matrix (RM) of the MPS with a PMC symmetry plane, $\bar{\mathbf{R}}_{\text{PEC}}$ is the RM of the MPS with a PEC symmetry plane, and $\bar{\mathbf{R}}$ is the RM of the mirror-symmetric MPS of Fig. 1(a). From (8), one can infer that

$$\bar{\mathbf{R}} = \frac{1}{2}(\bar{\mathbf{R}}_{\text{PMC}} + \bar{\mathbf{R}}_{\text{PEC}}) \quad (9)$$

Finally, let us subtract the excitation of the MPS in the presence of a PEC symmetry plane (Fig. 2(b)) from the excitation of the MPS in the presence of a PMC symmetry plane (Fig. 2(a)). According to (1)-(5), the total impinging fields existing in the upper half-space and the lower half-space of the mirror-symmetric MPS of Fig. 1(a) will be given by

$$\mathbf{E}_{\text{inc}}(\mathbf{r}) = \mathbf{0}, \quad \mathbf{H}_{\text{inc}}(\mathbf{r}) = \mathbf{0}, \quad z > 0 \quad (10)$$

$$\mathbf{E}_{\text{im}}(\mathbf{r}) = 2\mathbf{E}_{\text{im}}^{\text{PMC}}(\mathbf{r}), \mathbf{H}_{\text{im}}(\mathbf{r}) = 2\mathbf{H}_{\text{im}}^{\text{PMC}}(\mathbf{r}), \quad z < -2d_0 \quad (11)$$

Eqns. (10)-(11), opposite to (6)-(7), indicate that in the case of subtraction of the excitations, the incident plane waves from the upper half-space $z > 0$ of Figs. 2(a) and 2(b) cancel each other, but the *image* incident waves from the lower half-space $z < -2d_0$ add constructively. The resulting situation is that of an impinging wave from the lower half-space $z < -2d_0$ on the whole mirror-symmetric MPS of Fig. 1(a). Although this may seem different from the situation where the wave impinges from the upper half-space $z > 0$, both situations are essentially the same owing to the existence of the symmetry plane of the MPS at $z = -d_0$. This means that the fields of the wave transmitted to the upper half-space $z > 0$ by the incident wave impinging from the lower half-space $z < -2d_0$ after scattering by the MPS (once again, we assume grating lobes are not excited) can be obtained in terms of the fields of the waves reflected to the upper half-space $z > 0$ in the two situations (PMC and PEC at the bottom of the semi-MPS) of Fig. 1(b) by invoking again the superposition principle. In fact, the complex amplitudes of the components of the electric field of the transmitted wave parallel to the symmetry plane in

Fig. 1(a) (E_{0x}^t, E_{0y}^t) can be obtained in terms of the complex amplitudes of the components of the incident image electric field parallel to the symmetry plane by means of the expression

$$\begin{pmatrix} E_{0x}^t \\ E_{0y}^t \end{pmatrix} = \bar{\mathbf{R}}_{\text{PMC}} \cdot \begin{pmatrix} \frac{1}{2}E_{0x}^i \\ \frac{1}{2}E_{0y}^i \end{pmatrix} + \bar{\mathbf{R}}_{\text{PEC}} \cdot \begin{pmatrix} -\frac{1}{2}E_{0x}^i \\ -\frac{1}{2}E_{0y}^i \end{pmatrix} \\ = \left(\frac{1}{2}\bar{\mathbf{R}}_{\text{PMC}} - \frac{1}{2}\bar{\mathbf{R}}_{\text{PEC}} \right) \cdot \begin{pmatrix} E_{0x}^i \\ E_{0y}^i \end{pmatrix} = \bar{\mathbf{T}} \cdot \begin{pmatrix} E_{0x}^i \\ E_{0y}^i \end{pmatrix} \quad (12)$$

where $\bar{\mathbf{T}}$ is the transmission matrix (TM) of the whole mirror-symmetric MPS of Fig. 1(a). As a result of (12), we can write:

$$\bar{\mathbf{T}} = \frac{1}{2}(\bar{\mathbf{R}}_{\text{PMC}} - \bar{\mathbf{R}}_{\text{PEC}}) \quad (13)$$

Eqns. (9) and (13) both indicate that the electric field of the waves reflected and transmitted by the whole mirror-symmetric MPS of Fig. 1(a) can be exclusively obtained in terms of the electric field reflected by two semi-MPSs (half the size of the original whole MPS) of the type shown in Fig. 1(b), the first one with a PMC at its bottom, and the second with a PEC at its bottom. This indicates that the solution of the scattering problem for the MPS in Fig. 1(a), in practice numerically discretized in a given number of unknowns, can be substituted by the solution of two simpler scattering problems for the semi-MPS in Fig. 1(b), each of which must be discretized in half the number of unknowns of the original problem. This strategy is expected to provide an important overall CPU time saving, as will be shown in Section III.

B. Spectral-domain Green's functions for MPSs

SD-MoM [1] is a popular numerical technique for the analysis of the scattering by MPSs as that shown in Fig. 1(a). Unknowns are required to expand the 2D discrete Fourier transform (DFT) of the current density $\tilde{\mathbf{J}}_q$ [7, Eqn. (5)], [17, Eqns. (3) & (10)] for every q th metallized interface where a patch lies and the 2D-DFT of the tangential electric field $\tilde{\mathbf{E}}_q$ [7, Eqn. (5)] for every q th metallized interface with an aperture (for the latter, the DFT of the magnetic current density can be used instead as shown in [17, Eqns. (4) & (11)]). As a matter of fact, adaption of an SD-MoM code meant for free-space standing MPSs as the one shown in Fig. 1(a) to the case of MPSs with a PMC or a PEC at their bottom only requires two modifications: 1) computing the analytical solution to the scattering by the multilayered structure with no metallizations and 2) introducing new expressions for the 2D-DFTs of the dyadic Green's functions. Change n. 1 is trivial, while change n. 2 will be developed next.

Assuming an MPS with Q metallized interfaces, according to [7, Eqn. (1)] and [18, Eqn. (5)], there is a matrix relation between the 2D-DFTs of the current densities on the metallized interfaces, $\tilde{\mathbf{J}}_q$, and the tangential electric field at those interfaces, $\tilde{\mathbf{E}}_q$ ($q = 1, \dots, Q$), which can be written synthetically as

$$\tilde{\mathbf{J}}_Q = \tilde{\mathbf{L}}_{Q,Q} \cdot \tilde{\mathbf{E}}_Q + \tilde{\mathbf{L}}_{Q,Q-1} \cdot \tilde{\mathbf{E}}_{Q-1} \quad (14)$$

$$\tilde{\mathbf{J}}_q = \tilde{\mathbf{L}}_{q,q+1} \cdot \tilde{\mathbf{E}}_{q+1} + \tilde{\mathbf{L}}_{q,q} \cdot \tilde{\mathbf{E}}_q + \tilde{\mathbf{L}}_{q,q-1} \cdot \tilde{\mathbf{E}}_{q-1} \quad (15)$$

$(q = 2, \dots, Q-1)$

$$\tilde{\mathbf{J}}_1 = \tilde{\mathbf{L}}_{1,2} \cdot \tilde{\mathbf{E}}_2 + \tilde{\mathbf{L}}_{1,1} \cdot \tilde{\mathbf{E}}_1 \quad (16)$$

where the metallization number q of an MPS is ordered from the lowermost $q = 1$ to the uppermost $q = Q$ metallization level, as shown either in Fig. 1(a) or Fig. 1(b) ($Q = Q_{\text{tot}}$ in Fig. 1(a) and $Q = Q_{\text{half}}$ in Fig. 1(b)).

In the case of MPSs with alternating patches and apertures such as those of Figs. 1(a) and 1(b), the required spectral dyadic Green's functions for the application of the SD-MoM have to be obtained in terms of the 2×2 spectral matrices $\bar{\mathbf{L}}_{i,j}$ ($i, j = 1, \dots, Q$) of (14)-(16) as reported in [7, Eqns. (3) & (4)]. These $\bar{\mathbf{L}}_{i,j}$ matrices can be computed by means of the recurrent algorithm described in [18]. The values of $\bar{\mathbf{L}}_{1,1}$, $\bar{\mathbf{L}}_{2,2}$ and $\bar{\mathbf{L}}_{1,2} = \bar{\mathbf{L}}_{2,1}$ are critical to analyze both MPSs shown in Figs. 1(a) and 1(b), since these values are used as starting point in this recurrent algorithm. In particular, if the interface located at the bottom of the MPS ($q = 1$) is an interface with free space as shown in Fig. 1(a) (in this case the bottom interface is the plane $z = -2d_0$), then matrices $\bar{\mathbf{L}}_{i,j}$ ($i, j = 1, 2$) of (14)-(16) are given by

$$\bar{\mathbf{L}}_{1,1} = -j\omega\epsilon_0 \left\{ \frac{\bar{\mathbf{M}}_1}{\Omega_1} \coth(\Omega_1 h_1) + \frac{\bar{\mathbf{M}}_0}{\Omega_0} \right\} \quad (17)$$

$$\bar{\mathbf{L}}_{1,2} = \bar{\mathbf{L}}_{2,1} = j\omega\epsilon_0 \frac{\bar{\mathbf{M}}_1}{\Omega_1} \text{csch}(\Omega_1 h_1) \quad (18)$$

$$\bar{\mathbf{L}}_{2,2} = -j\omega\epsilon_0 \left\{ \frac{\bar{\mathbf{M}}_2}{\Omega_2} \coth(\Omega_2 h_2) + \frac{\bar{\mathbf{M}}_1}{\Omega_1} \coth(\Omega_1 h_1) \right\} \quad (19)$$

where

$$\bar{\mathbf{M}}_i = \begin{pmatrix} \epsilon_{ri} - \frac{(k_{yn})^2}{k_0^2} & \frac{k_{xm}k_{yn}}{k_0^2} \\ \frac{k_{xm}k_{yn}}{k_0^2} & \epsilon_{ri} - \frac{(k_{xm})^2}{k_0^2} \end{pmatrix} \quad (i = 0, 1, 2) \quad (20)$$

$$\Omega_i = \sqrt{(k_{xm})^2 + (k_{yn})^2 - k_0^2 \epsilon_{ri}} \quad (i = 0, 1, 2) \quad (21)$$

and where $\epsilon_{r0} = 1$. In the case of the periodic rectangular lattice treated in this paper, the spectral variables k_{xm} and k_{yn} of (20) and (21) are $k_{xm} = k_0 \sin \theta_{\text{inc}} \cos \varphi_{\text{inc}} + (2\pi m)/D_x$ and $k_{yn} = k_0 \sin \theta_{\text{inc}} \sin \varphi_{\text{inc}} + (2\pi n)/D_y$. However, the results of this paper can be extended to periodic skewed lattices, and in this latter case, the spectral variables have to be redefined as shown in [7, Eqns. (8) & (9)].

Now, if we consider MPSs as those shown in Fig. 1(b), where metallization level $q = 1$ coincides either with a PMC or a PEC, located at the bottom of the MPS (in this case, plane $z = -d_0$), matrices $\bar{\mathbf{L}}_{i,j}$ ($i, j = 1, 2$) of (14)-(16), used as the starting point for the aforementioned recurrent algorithm, have to be redefined as [15]

$$\bar{\mathbf{L}}_{1,1} = \bar{\mathbf{L}}_{1,2} = \bar{\mathbf{L}}_{2,1} = \bar{\mathbf{0}} \quad (22)$$

$$\bar{\mathbf{L}}_{2,2} = -j\omega\epsilon_0 \left\{ \frac{\bar{\mathbf{M}}_2}{\Omega_2} \coth(\Omega_2 h_2) + \frac{\bar{\mathbf{M}}_1}{\Omega_1} \tanh(\Omega_1 h_1) \right\} \quad (23)$$

(PMC at the bottom)

$$\bar{\mathbf{L}}_{2,2} = -j\omega\epsilon_0 \left\{ \frac{\bar{\mathbf{M}}_2}{\Omega_2} \coth(\Omega_2 h_2) + \frac{\bar{\mathbf{M}}_1}{\Omega_1} \coth(\Omega_1 h_1) \right\} \quad (24)$$

(PEC at the bottom)

Replacement of (17)-(19) by (22)-(24) in (14)-(16) ensures that the SD-MoM can be applied when the MPS of Fig. 1(b) is limited at the bottom by a PMC/PEC instead of being limited by an interface with free space (as the MPS of Fig. 1(a)).

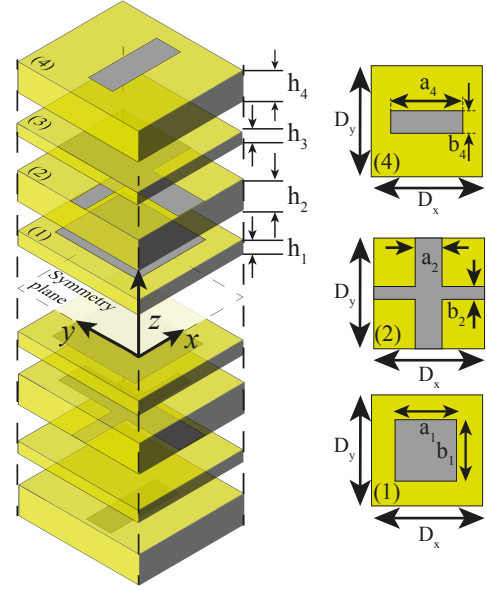


Fig. 3. Unit cell of the designed LP-to-CP converter.

III. NUMERICAL APPLICATION EXAMPLE

The theory presented in Section II has been exploited to design an LP-to-CP converter of the type described in [8]. Fig. 3 shows the unit cell of the LP-to-CP converter. The converter is an MPS with a symmetry plane containing six metallization levels, four of them made of periodic arrays of rectangular patches and two of them made of periodic arrays of rectangular apertures. The six metallization levels are separated by seven dielectric layers. Three of the dielectric layers are bonding layers of Rogers 4450F prepreg material (with thickness 0.1 mm and dielectric constant 3.52), and the remaining four layers correspond to Rogers RT/Duroid 6010 (with two different thicknesses 0.635 mm and 1.27 mm, and dielectric constant 10.2). All seven dielectric layers of the MPS (including the bonding layers) are commercially available substrates as shown in [8]. In accordance with [8, Fig. 4], the MPS including the patches and apertures acts as a broadband passband filter with very linear phase response for the x and y components of the impinging electric field under normal incidence. The transmission windows of these two components do not coincide, but there is an overlapping frequency interval in which a constant 90° difference can be achieved in the transmission phase, which yields broadband circular polarization in that overlapping range of frequency.

In order to design the LP-to-CP converter, we have analyzed the unit cell of Fig. 3 using the procedure of Section II. The analysis of these two unit cells limited by PMC/PEC has been carried out by means of SD-MoM while using (22) to (24) in (14)-(16) for the computation of the spectral dyadic Green's functions.

The band chosen for the operation of the designed LP-to-CP converter is that between 11.5 and 14.5 GHz (center frequency 13 GHz) which includes both the TX and RX bands of a real Ku-band telecommunication mission [19]. A cost function has been defined that optimizes the values of the geometrical dimensions a_i y b_i ($i = 1, 2, 4$) of Fig. 3 to minimize the axial

TABLE I
SUBSTRATE LAYER PARAMETERS AND METALLIZATIONS DIMENSIONS IN
THE DESIGNED LP-TO-CP CONVERTER

Parameter	h_1	h_2	h_3	h_4
Value	0.05 mm	0.635 mm	0.1 mm	1.27 mm
Parameter	ϵ_{r1}	ϵ_{r2}	ϵ_{r2}	ϵ_{r4}
Value	3.52	10.2	3.52	10.2

Parameter	D_x	D_y	a_1	b_1
Value	3.29 mm	3.29 mm	2.57 mm	1.50 mm
Parameter	a_2	b_2	a_4	b_4
Value	0.66 mm	0.1 mm	1.73 mm	0.50 mm

ratio of the wave transmitted by the unit cell when an LP wave impinges on the cell with electric field at 45° with axes x e y under normal incidence conditions, and simultaneously maximize the transmission of the x and y components of the electric field of this incident wave, also under normal incidence conditions. Both the minimization of the axial ratio and the maximization of the transmission have been enforced throughout the operation band between 11.5 and 14.5 GHz. The resulting optimized dimensions of the metallizations of the unit cell are shown in Table I. The total CPU time consumption needed to reach the optimized dimensions with our in-house SD-MoM software was roughly of 280 seconds (around 1500 different SD-MoM problems limited by both PMC and PEC were analyzed), and the optimization method employed was the locally biased variant of the global optimization algorithm DIRECT [20] for which routines can be found in [21]. All simulations were run on a computer with a CPU AMD Ryzen Threadripper PRO 3995WX sWRX8 2.7 GHz and 128 GB RAM. The operating system is Windows 10 Pro 21H2 (64-bit).

Figs. 4(a) and 4(b) show the results obtained for the designed LP-to-CP converter under normal incidence conditions for the axial ratio of the transmitted wave, and for the transmission of the two components of the incident electric field (T_x y T_y are the diagonal coefficients of the transmission matrix \mathbf{T}_{ep} defined en (13)). Note the axial ratio is roughly below 1 dB and the transmission above -1 dB in the whole operation band. The MoM results are compared with CST results, and good agreement is found. In the case of Fig. 4(a), we plot CST results obtained for the whole multilayered structure as well as CST results obtained with the two semi-structures limited by PMC and PEC with excellent agreement. We have found a 42% CPU time reduction in CST when symmetry is exploited as explained in Section II. With our in-house SD-MoM software, the CPU time required is around 0.70 seconds per frequency point for the analysis of the whole MPS, and around 0.21 seconds per frequency point for the two semi-structures, leading to a 30% CPU time reduction. The two orders of magnitude CPU time difference between CST and SD-MoM justifies the use of in-house software instead of commercial software for design purposes. Figs. 5(a) to 5(d) show results for the axial ratio and the transmission of the LP-to-CP converter under oblique incidence conditions. Good agreement is again found between the SD-MoM results as applied to the two semi-structures limited by PMC and PEC

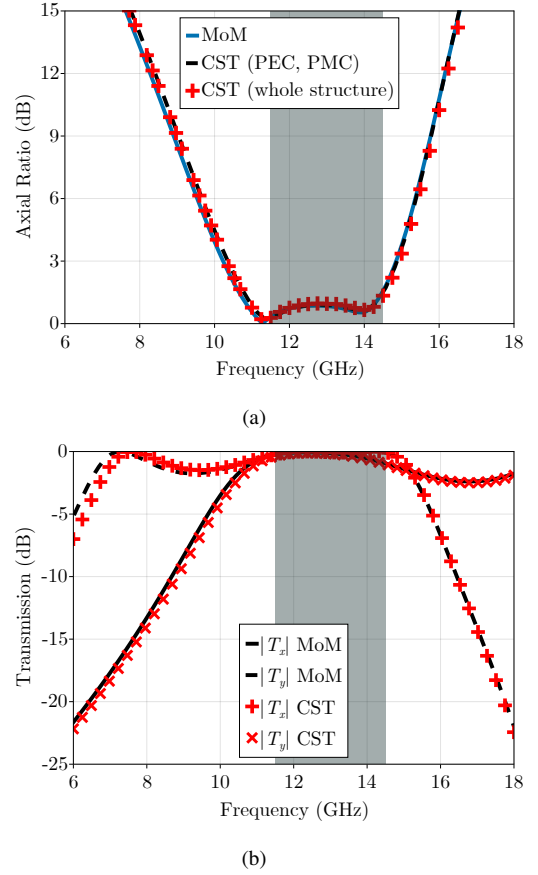


Fig. 4. Axial ratio (a) and transmission characteristics (b) of the LP-to-CP converter of Fig. 3 under normal incidence conditions when the substrate layers and dimensions of Table I are used.

and the results of CST as applied to the whole MPS, which again validates the theory of Section II for oblique incidence. Note that the optimized properties of the LP-to-CP converter are preserved to a large extent (axial ratio below 2.5 dB and transmission above -1 dB) when angle of incidence θ_{inc} increases as previously shown for miniaturized-element FSS, which ensures a robust performance of the converter for a wide range of angles of incidence [8].

IV. CONCLUSION

The authors have shown that the analysis of an MPS with a symmetry plane can be split into the analysis of two semi-structures in which the symmetry plane behaves either as a PMC or as a PEC. Both in-house software based on the SD-MoM and commercial software CST have been used to prove the equivalence between the analysis of the whole MPS and the analysis of the two semi-structures, the analysis of the two semi-structures requiring a CPU time which is between 30% and 42% shorter than that required by the analysis of the whole MPS. This demonstrates the CPU time saving in the numerical analysis of mirror-symmetric MPSs when symmetry is exploited.

REFERENCES

- [1] R. Mittra, C. H. Chan, and T. Cwik, "Techniques for analyzing frequency selective surfaces—A review," *Proc. IEEE*, vol. 76, no. 12, pp. 1593-1615, Dec. 1988.

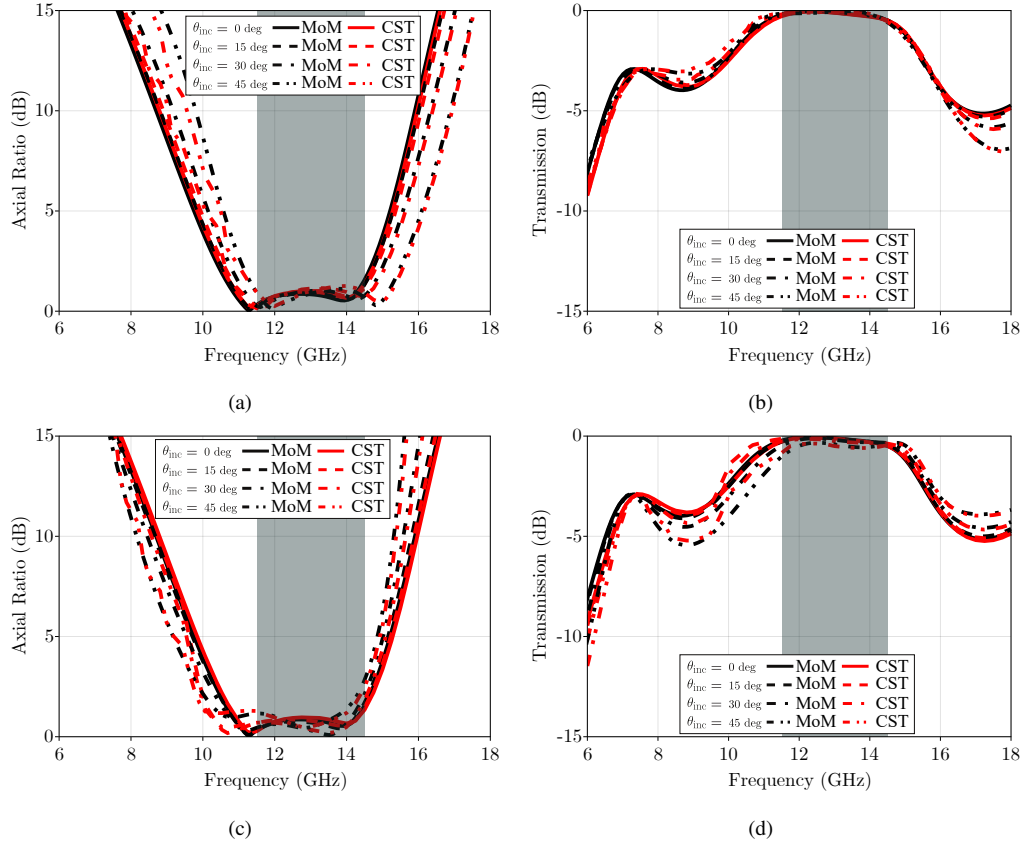


Fig. 5. Axial ratio ((a) and (c)) and transmission characteristics ((b) and (d)) of the LP-to-CP converter of Fig. 3 under normal and oblique conditions when the substrate layers and dimensions of Table I are used. Cases (a) and (b) correspond to oblique incidence in the x - z plane ($\varphi_{\text{inc}} = 0^\circ$), and cases (c) and (d) correspond to oblique incidence in the y - z plane ($\varphi_{\text{inc}} = 90^\circ$).

- [2] B. A. Munk, *Frequency Selective Surfaces: Theory and Design*. New York, NY, USA: Wiley, 2000.
- [3] N. Behdad, M. A. Al-Joumayly, and M. Salehi, "A low-profile third-order bandpass frequency selective surface," *IEEE Trans. Antennas Propagat.*, vol. 57, no. 2, pp. 460-466, Feb. 2009.
- [4] N. Behdad and M. A. Al-Joumayly, "A generalized synthesis procedure for low-profile, frequency selective surfaces with odd-order bandpass responses," *IEEE Trans. Antennas Propagat.*, vol. 58, no. 7, pp. 2460-2464, July 2010.
- [5] M. A. Al-Joumayly and N. Behdad, "A generalized method for synthesizing low-profile, band-pass frequency selective surfaces with non-resonant constituting elements," *IEEE Trans. Antennas Propagat.*, vol. 58, no. 12, pp. 4033-4041, Dec. 2010.
- [6] M. A. Al-Joumayly and N. Behdad, "Low-profile, highly-selective, dual-band frequency selective surfaces with closely spaced bands of operation," *IEEE Trans. Antennas Propagat.*, vol. 58, no. 12, pp. 4042-4050, Dec. 2010.
- [7] J. Corcoles and R. R. Boix, "Spectral MoM NUFFT-based formulation for the efficient analysis of high-order bandpass FSSs with tightly packed non-resonant elements in skewed grid," *IEEE Trans. Antennas Propagat.*, vol. 69, no. 9, pp. 6099-6104, Sept. 2021.
- [8] S. M. A. M. H. Abadi and N. Behdad, "Wideband linear-to-circular polarization converters based on miniaturized-element frequency selective surfaces," *IEEE Trans. Antennas Propagat.*, vol. 64, no. 2, pp. 525-534, Feb. 2016.
- [9] M. Hosseini and S. H. Hum, "A circuit-driven design methodology for a circular polarizer based on modified Jerusalem cross grids," *IEEE Trans. Antennas Propagat.*, vol. 65, no. 10, pp. 5322-5331, Oct. 2017.
- [10] D. Blanco and R. Sauleau, "Broadband and broad-angle multilayer polarizer based on hybrid optimization algorithm for low-cost Ka-band applications," *IEEE Trans. Antennas Propagat.*, vol. 66, no. 4, pp. 1874-1881, April 2018.
- [11] G. Pérez-Palomino, Juan E. Page, M. Arrebola and J. A. Encinar, "A design technique based on equivalent circuit and coupler theory for broadband linear to circular polarization converters in reflection or transmission mode," *IEEE Trans. Antennas Propagat.*, vol. 66, no. 5, pp. 2428-2438, May 2018.
- [12] H. B. Wang and Y. J. Cheng, "Single-layer dual-band linear-to-circular polarization converter with wide axial ratio bandwidth and different polarization modes," *IEEE Trans. Antennas Propagat.*, vol. 67, no. 6, pp. 4296-4301, Jun. 2019.
- [13] M. Del Mastro, M. Ettorre and A. Grbic, "Dual-band orthogonally-polarized LP-to-CP converter for SATCOM applications," *IEEE Trans. Antennas Propagat.*, vol. 68, no. 9, pp. 6764-6776, Sept. 2020.
- [14] D. M. Pozar, *Microwave Engineering*, Fourth Edition, Hoboken, NJ, USA: Wiley, 2012, ch. 7.
- [15] F. Medina, M. Horno and H. Baudrand, "Generalized spectral analysis of planar lines on layered media including uniaxial and biaxial dielectric substrates," *IEEE Trans. Microwave Theory Tech.*, vol. 37, no. 3, pp. 504-511, March 1989.
- [16] A. Altaf, H. Sajjad, C. Ozzaim and E. Arvas, "Scattering from chiral cylinders of arbitrary cross-sections above a ground plane," *IEEE Access*, vol. 9, pp. 6735-6745, 2021.
- [17] M. Camacho, R. R. Boix and F. Medina, "NUFFT for the efficient spectral domain MoM analysis of a wide variety of multilayered periodic structures," *IEEE Trans. Antennas Propagat.*, vol. 67, no. 10, pp. 6551-6563, Oct. 2019.
- [18] F. Mesa, R. Marqués and M. Horno, "A general algorithm for computing the bidimensional spectral Green's dyad in multilayered complex bianisotropic media: the equivalent boundary method," *IEEE Trans. Microwave Theory Tech.*, vol. 39, no. 9, pp. 1640-1649, Sept. 1991.
- [19] J. A. Encinar, M. Arrebola, Luis F. de la Fuente and G. Toso, "A transmit-receive reflectarray antenna for direct broadcast satellite applications," *IEEE Trans. Antennas Propagat.*, vol. 67, no. 10, pp. 3255-3264, Sept. 2011.
- [20] J. M. Gablonsky and C. T. Kelley, "A Locally Biased form of the DIRECT algorithm," *J. Global Optimization*, vol. 21, no. 1, pp. 27-37, 2001.
- [21] Steven G. Johnson, "The NLOpt non-linear optimization package", Internet: <http://github.com/stevengj/nlopt> (accessed April 28th 2023)